Efficient Directed Energy Transfer through Size-Gradient Nanocrystal Layers into Silicon Substrates

*William J. I. De Benedetti, Michael T. Nimmo, Sara M. Rupich, Louis M. Caillard, Yuri N. Gartstein, Yves J. Chabal and Anton V. Malko**

Spectroscopic evidence of directed excitonic energy transfer (ET) is presented through size-gradient CdSe/ZnS nanocrystal quantum dot (NQD) layers into an underlying Si substrate. NQD monolayers are chemically grafted on hydrogen-terminated Si surfaces via a self-assembled monolayer of amine modified carboxy-alkyl chains. Subsequent NQD monolayers are linked with short alkyldiamines. The linking approach enables accurate positioning and enhanced passivation of the layers. Two different sizes of NQDs (energy donors emitting at 545 nm, and energy acceptors emitting at 585 nm) are used in comparing different monolayer and bilayer samples grafted on SiO_2 and oxide-free Si surfaces via time-resolved photoluminescence measurements. The overall efficiency of ET from the top-layer donor NQDs into Si is estimated to approach ≈90% through a combination of different energy relaxation pathways. These include sequential ET through the intermediate acceptor layer realized mainly via the non-radiative mechanism and direct ET into the Si substrate realized by means of the radiative coupling. The experimental observations are quantitatively rationalized by the theoretical modeling without introducing any extraneous energy scavenging processes. This indicates that the linker-assisted fabrication enables the construction of defect-free, bandgap-gradient multilayer NQD/Si hybrid structures suitable for thin-film photovoltaic applications.

1. Introduction

There has been a significant interest in nanostructured photovoltaics[1] as a broad platform that can potentially enable cost-effective production of efficient and flexible solar cell modules. A multitude of structures utilizing different materials and architectures have been studied and while substantial progress has been achieved, their specific challenges and limitations are well recognized (see a well-referenced review article[1]). Since some of those limitations stem from the functional demands placed on the materials involved, it becomes important to understand if those demands could be alleviated by employing different operational principles. Such an opportunity may arise in energy transfer (ET) based hybrid nanostructures[2,3] that seek a clear separation of the functionalities of the different materials components: one component of the hybrid structure is chosen for its strong light-matter interaction while the other for its high charge-carrier mobilities. The strong near-field electromagnetic interaction is responsible for inter-conversion of neutral excitations, excitons and electron-hole pairs, between the components. In the photovoltaic (PV) mode of operation, solar light is harvested in the highly absorbing component followed by exciton diffusion and ET across the interface with the subsequent separation and transport of charge carriers entirely within the high-mobility semiconductor component. This separation of functionalities is conceptually reminiscent of photosynthesis,[4] where solar energy is absorbed in light-harvesting antennae and then relayed to reaction centers that enable charge separation. Hybrid architectures operating on ET principles should thus be contrasted with conventional[1] charge transfer based PV nanostructures. Many charge transfer based structures, for example, rely on exciton fission at the interface resulting in charge carriers on both sides and therefore place high demands on carrier mobilities in both components as well as on the microscopic quality of the interface.

We have recently shown[5,6] that a combination of colloidal nanocrystal quantum dots (NQDs) with ultrathin crystalline Si layers could be an attractive practical realization of ET-based hybrids for thin-film solar cells that would take advantage of the beneficial properties of both components. On the one hand, Si layers in such devices are effectively sensitized via ET from NQDs. Hence, the issue of weak solar light absorption in Si is no longer a defining factor in the overall design of the solar cell and the thickness of the crystalline Si layer can be substantially reduced to fractions of a micron in our experiments.[5] On the other hand, NQDs, well-known as good light absorbers and emitters, are no longer required to exhibit good charge carrier transport in their assemblies. We have experimentally demonstrated very efficient (close to 90%) ET coupling between individual proximal NQDs and Si substrates over a wide spectral

W. J. I. De Benedetti, Dr. S. M. Rupich, L. M. Caillard, Prof. Y. J. Chabal
Department of Materials Science and Engineering
The University of Texas at Dallas
Richardson, Texas 75080, USA
M. T. Nimmo, Prof. Y. N. Gartstein, Prof. A. V. Malko
Department of Physics
The University of Texas at Dallas, EC36
Richardson, Texas 75080, USA
E-mail: anton.malko@utdallas.edu

DOI: 10.1002/adfm.201400667

range as enabled via both non-radiative (NRET) and radiative (RET) mechanisms.[5–8] Hybrid structures with ET coupling can also be realized in different three-dimensional geometries.[9–11] Given the maturity of Si technology and chemical processability of colloidal NQDs, NQD/Si hybrid structures are expected to be manufacturable without major new developments.

Further assessment of the practical viability of NQD/Si hybrids requires fabrication and analysis of energy flows in structures with optically thick, multi-layer NQD arrays that would provide sufficient absorption of the incident solar light. While significant research has been carried out on various "NQD solids" due to the NQD's unique physicochemical properties of band-gap tunability, photostability and solution processability attractive for optoelectronic applications, most of the effort has focused on the improvement of carrier mobilities in these arrays.[12] For example, lead chalcogenide NQDs have been employed in conventional PV nanostructures[1,13] due to their superior performance in the near-infrared (NIR) spectral region in comparison with organic dyes; however, low charge carrier mobilities hinder progress in such NQD based solar cells. While sharing the requirement of good light absorption with conventional architectures, ET-based structures, in contrast, do not use charge transport within the NQD arrays and therefore are amenable to different property optimizations.

It is worthwhile to recall that charge and energy transfer processes have very different relevant spatial scales. Charge transfer relies on the overlap of the electronic wave functions and is therefore determined by angstrom-scale interactions; the ligands on NQDs can strongly influence charge transport in NQD solids. On the other hand, ET processes rely on relatively long-range electromagnetic interactions: the typical length scales are several nanometers for NRET and are even longer ranged for radiative transfer processes. RET from NQDs into Si substrates is expected to be efficient over distances of tens of nanometers.[5,6,8]

One of the important requirements for assembling NQDs in our structures is to minimize the number of energy (exciton) scavenging events and thereby preserve their high quantum yields (QYs). This is a significant practical issue as it is known that the deposition of densely-packed NQD films commonly leads to substantial reductions in the photoluminescence (PL) QYs as compared to QYs in solutions.[14] Contributing to the deterioration of the PL QY in dense arrays is the NRET-mediated diffusion of excitons towards "defective" NQDs that act as excitonic traps where "dark-state" excitations are irrecoverably lost. One can envision various approaches to battle such energy losses. The direct approach is the reduction of the dark-exciton traps by appropriate chemical and growth routes that would tightly control the resulting structure and passivate defect sites. Recent work[15] demonstrating low-threshold lasing with dense NQD films illustrates that issues of high-QY arrays can be successfully addressed via proper fabrication.

One can also utilize accelerated directed migration of excitons from their generation locations towards the high-mobility semiconductor substrate. This design would mitigate exciton scavenging that is more frequently encountered in the random diffusion process. The idea of exciton drift can be naturally pursued in assemblies with engineered NQD size (band-gap) gradients. Indeed, several groups have demonstrated this effect in bilayer[16] and multilayer[17,18] configurations where different size NQDs are arranged in layer-by-layer geometries on neutral glass substrates. Since quantum confinement in NQDs results in larger exciton energy for smaller diameter dots (of the same composition), the NRET processes enable fast directed migration of relaxed excitons towards the layer with the largest dots. While short interlayer NRET times of fractions of a nanosecond were reported, the graded films in previous studies[16–18] were not optimized to maintain high overall QYs and no attempts were made to convert excitons into accessible excitations inside conducting media.

In this paper, we explore these two approaches *via* a detailed spectroscopic study of energy relaxation pathways in size-gradient, dense NQD bilayer structures carefully grafted on planar Si and SiO_2 substrates. NQD grafting via self-assembled monolayers (SAMs) of functionalized molecules assures both the electronic purity of the underlying substrate[19] and the uniform placement of NQDs allowing for the ET processes to be studied unobscured. Additionally, the linker strategy enables us to carefully build up the subsequent NQD monolayers in a controlled manner. By using time-resolved PL measurements of the donor and acceptor NQD emission, we find that energy is unidirectionally transported into the Si substrate via sequential exciton NRET migration and direct RET coupling to the Si substrate. Based on the analysis of the experimentally measured ET times between NQD layers and Si substrates, we estimate the overall transfer efficiency of the donor excitons in the outmost layer into Si substrate approaching ≈90%. Our measurements and observations are in a good agreement with theoretical analysis of NRET- and RET-mediated energy transport in the absence of detrimental energy-scavenging mechanisms. These results suggest that linker-assisted assembly can enable the fabrication of defect-free NQD multilayer structures with unimpeded energy flows into the underlying semiconductor substrate. This further supports the concept of ET-based hybrid nanocrystal/Si thin film PV devices, where bandgap-engineered optically thick NQD layers are used as primary solar photon absorbers to further funnel excitons into high-charge-mobility ultrathin Si substrates.

2. Results and Discussion

We studied and compared the time-resolved decay of excitons in photoexcited NQDs in monolayer and bilayer arrangements on SiO_2 and Si substrates as schematically shown in **Figure 1**a and 4a. NQD monolayers were attached to the substrates via amine terminated SAMs. In the bilayer samples, a second layer of NQDs was linked to an underlying monolayer of NQDs via short alkyldiamines. We have used two different sizes of CdSe/ZnS core shell NQDs, whose PL emission spectra are centered approximately at 545 nm and at 585 nm. We refer to them as donor (D) and acceptor (A) NQDs, respectively, as they act in the capacity of energy donors and energy acceptors in the bilayer configuration. The experimental PL data for NQDs on SiO_2 substrates are collected in Figure 1 and the data for NQDs on Si substrates in Figure 4. With the selected NQDs, the emission spectra of Ds and As are well separated as is clear from the figures. Moreover, the ca. 0.16 eV difference in energy of the

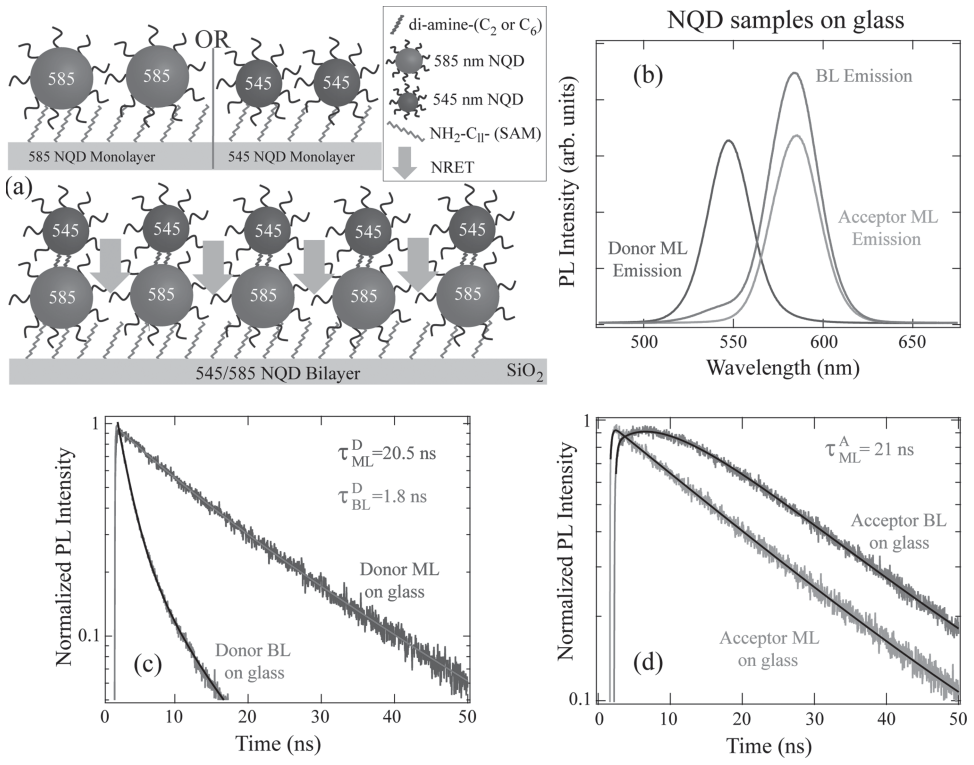

Figure 1. a) Schematics of the monolayer and bilayer placement on SiO_2 substrate. b) PL emission spectra for donor monolayer (NQD-545, ML), acceptor monolayer (NQD-585, ML) and bilayer (NQD-545 on NQD-585, BL) samples grafted on SiO_2. The spectra represent three different samples. c) PL dynamics at donor emission peak (545 nm) for donor monolayer (top trace) and bilayer (bottom trace) samples. Traces are shown along with the fitting curves. d) PL dynamics at acceptor emission peak (585 nm) for acceptor monolayer (bottom trace) and bilayer (top trace) samples. Fitting curves are also displayed for panels (c) and (d).

respective excitons is large enough to prevent thermally activated exciton transfer from A to D at room temperature. Under this condition, the simplest linear kinetic model describing the time evolution of the number of donor, N_D, and acceptor, N_A, excitons from their original quantities $N_D(0)$ and $N_D(0)$ at time $t = 0$ is given by equations:[20]

$$\frac{dN_D}{dt} = -\gamma^D N_D - wN_D; \quad (1)$$

$$\frac{dN_A}{dt} = -\gamma^A N_A + wN_D. \quad (2)$$

Here, w is the rate of the exciton transfer from the excited donor NQD to the acceptor NQDs, while γ^D and γ^A are the decay rates of the D and A excitons due to all other radiative and non-radiative processes. (It should be kept in mind that γ^D and γ^A rates can themselves depend on the configuration under study.) The solutions to Equation (1) and (2):

$$N_D(t) = N_D(0)e^{-(\gamma^D + w)t}, \quad (3)$$

$$N_A(t) = N_A(0)e^{-\gamma^A t} + \frac{wN_D(0)}{\gamma^D + w - \gamma^A}(e^{-\gamma^A t} - e^{-(\gamma^D + w)t}), \quad (4)$$

can be exploited in the analysis of the experimental data in the bilayer samples. When compared with the PL dynamics of the monolayers, the important qualitative features of the solutions are the acceleration of the D decay in Equation (3) due to exciton transfer to A (here it is a mono-exponential decay), and the appearance of the corresponding energy "in-flow" in the acceptor dynamics in Equation (4). These salient features are exhibited by the experimental data in panels (c) and (d) of Figure 1.

Figure 1b shows the PL spectra of D and A emission in monolayer and bilayer samples grafted on SiO_2 substrates. It is clearly seen that in the bilayer sample, the relative PL intensity from the donor NQDs is much smaller than the PL from the acceptor NQDs. This is indicative of efficient ET from the donor to the acceptor layer as characteristic of short-distance NRET processes.[18] It may be unreliable to make quantitative assessments of the efficiency and rates of the NRET process from PL intensity (or photon count) measurements as, for instance, varying NQD surface coverage would inherently affect the comparison between samples. A direct and much more reliable quantitative approach is to study changes in the PL dynamics which are unaffected by the number of photo-excitations and rather are determined only by the rates of the relevant processes.[8] Figure 1c shows a drastic acceleration of the donor PL intensity decay in the presence of acceptors in the bilayer configuration (bottom trace, BL) as compared to the donor decay in the monolayer configuration (top trace, ML): the respective

decay times are found as τ_{BL}^{D} = 1.8 ns and τ_{ML}^{D} = 20.5 ns. The faster donor PL decay in the bilayer structure clearly demonstrates the presence of an additional decay channel, which is NRET from the donor to the acceptor layer. A good estimate of the interlayer rate w can be derived already from the raw data. Indeed, in the case of the SiO_2 substrates, the D decay rate γ^{D} into other channels can be approximated by its value $\gamma_{ML}^{D} = 1/\tau_{ML}^{D}$ in the donor monolayer configuration. This arises from the fact that these other decay channels for samples on the SiO_2 substrate are presumed to be purely radiative.[5,6] The distance from the donor layer to the SiO_2 substrate in the bilayer, while larger than in the donor monolayer, is still only about 10 nm so that the change in the donor radiative rates between the bilayer and monolayer samples is small.[5,6] In this approximation, the interlayer NRET time $\tau_w = 1/w$ is then found from $w = 1/\tau_{BL}^{D} - 1/\tau_{ML}^{D}$ to be $\tau_w \cong 2.0$ ns. The efficiency of the interlayer NRET—defined as a fraction of the overall decay rate—is correspondingly evaluated as $w/(\gamma^{D} + w) = \tau_{BL}^{D}/\tau_w \cong 0.91$. This result strongly suggests that NRET from the donor to acceptor NQD layers is highly efficient. A more accurate analysis taking into account that bilayer's $\gamma < \gamma_{ML}^{D}$ would lead to a slightly shorter interlayer NRET time and a bit higher efficiency.

An important counterpart in the detection of the interlayer NRET is the observation of the energy "in-flow" in the A layer. To this aim, in Figure 1d we directly compare the time evolution of the PL of the acceptor layer in the bilayer structure (top trace, BL) to the PL of an acceptor monolayer on SiO_2 (bottom trace, ML), where no ET would occur. It is clearly seen that the A emission rises slower in the bilayer sample, consistent with ET from the D to A layer. For a clearer demonstration of the changes in the acceptor PL emission, we selected a bilayer sample with a somewhat higher concentration of donor NQDs. Indeed, as per Equation (4), changes in the rise time of the acceptor can be obscured if the initial number of excitons in the A layer, $N_A(0)$, is appreciably greater than the initial number $N_D(0)$ of donors excitons. Since the laser excitation of the donor NQDs also creates excitons in the acceptor NQDs and the absorption cross-section of the bigger-sized NQDs is larger, a larger number of excitons could be created in the acceptor layer. This is why samples with higher D concentrations are more desirable when probing acceptor rise times (Figure 1d).

While the simple kinetic Equation (1) and (2) feature single values of various rate constants resulting in the monoexponential D decay in Equation (3), the real samples are well known to frequently exhibit more variations. In fact, in several instances, we observed the presence a relatively weak second exponent in the D decay in bilayer structures as seen in Figure 1c. The second component may arise from a distribution of distances between the donor and acceptor NQDs, e.g. due to some small inhomogeneities in the NQD placement. In such cases, the experimental data is processed for fitting with weighted contributions from two rates: $w = C_1 w_1 + C_2 w_2$, where coefficients $C_{1,2}$ satisfy $C_1 + C_2 = 1$ and $w_{1,2}$ are NRET rates derived from biexponential fits to the donor decay traces.

The experimental traces in Figure 1 are overlayed with fitting curves from the kinetic model showing satisfactory agreement. In particular, the solid black curve in Figure 1d fits the acceptor dynamics in the bilayer configuration using Equation (4). All of the kinetic rate parameters for this equation (the donor and acceptor decay rates in the monolayers and the NRET rate in the bilayer) were first independently measured, thus leaving the relative initial number of D and A excitons, $N_D(0)/N_A(0)$, as a fit parameter. The displayed agreement between the model fit and experimental data is achieved for the ratio of $N_D(0)/N_A(0) \cong 1.2$. This value appears reasonable given the ratio of the D and A monolayer PL intensities in Figure 1b although we cannot make a direct comparison. The satisfactory quantitative characterization of the bilayer configuration on SiO_2 substrates can be used to extract information on the interlayer NRET interactions for analysis and comparisons with hybrid configurations on Si surfaces.

From Figure 1d, it is also clear that the acceptor exciton decay rates in the bilayer and monolayer configurations are very close: $\gamma^{A} \cong \gamma_{ML}^{A}$; moreover, the observed decay time of $\tau_{ML}^{A} \cong 21$ ns is very similar to the previously measured decays[6] in submonolayer samples. The latter observation is also true for the donor exciton decay in Figure 1c, where the measured decay time τ_{ML}^{D} closely matches our measurements in submonolayer samples. As the exciton decay in submonolayer samples is largely determined by the spontaneous decay rates of individual NQDs, our measurements of the PL kinetics in mono- and bilayers strongly indicate that no substantial detrimental exciton-scavenging channels were introduced when we fabricated dense NQD samples with our linking approach.

It is interesting and instructive to discuss the experimentally observed trends in the context of a related simpler theoretical model system which is depicted in **Figure 2**a. The theoretical analysis of the modification of the electromagnetic decay rate of an electric dipole emitter in the vicinity of stratified dissipative and non-dissipative substrates is well known[22,23] and we described details of its applications for similar systems in several recent publications.[5,6,8,24,25] Comparing exciton decay times τ_1 and τ_2 (without and with the acceptor layer, respectively) in model configurations of Figure 2a should be similar to comparing donor decay times τ_{ML}^{D} and τ_{BL}^{D} in the experimental monolayer and bilayer configurations. The computational results displayed in Figure 2b and 2c clearly illustrate how ET from the donor exciton into the acceptor layer is sensitively dependent on both the distance z to the layer and on the layer's dielectric/optical parameters n and a.

We show the results calculated for a range of values of these parameters that we expect to find in our experimental systems. The diameters of the NQDs used are about 4.7 nm and 5.3 nm for NQD-545 and NQD-585, respectively. The length of different linker molecules is assessed to be between 1 and 2 nm. The chemistry of our linkers ensures their direct attachment to the NQD body and to the substrate surface. One can thus estimate distances z from the centers of spherical NQDs (associated with the position of the point-like electric-dipole emitter) to the underlying (effective) surface.[6] For the effective absorption coefficient a of the acceptor layer that is treated in calculations as a continuum slab of thickness d = 5 nm, in **Figure 3** we also provide the results of our measurements on a monolayer of the acceptor NQDs. The experimentally measured optical density was converted here into the absorption coefficient assuming that the monolayer constitutes an absorbing slab of the same thickness d.

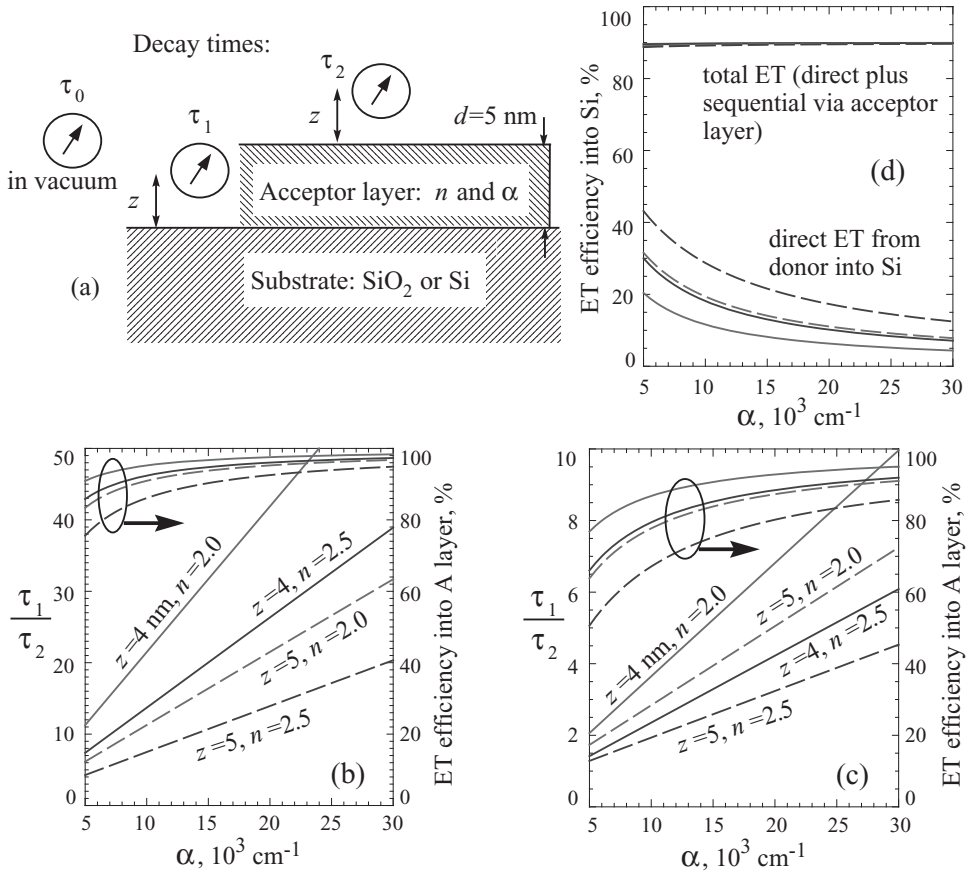

Figure 2. a) Schematics of a related simpler model system where a single randomly oriented electric-dipole donor exciton decays in different configurations: when in vacuum, its radiative decay time is τ_0, when in the vicinity (at distance z) of a substrate, the decay time is τ_1, and when at the same distance z from the acceptor layer on top of the same substrate, the decay time is τ_2. In calculations, the acceptor layer is a macroscopic slab of thickness $d = 5$ nm that is characterized by its absorption coefficient a and refraction index n. Panels (b) and (c) show the results of computations for the ratio of decay times τ_1/τ_2 as a function of the absorption coefficient a of the A layer in the model system. This ratio can be compared to experimental ratios τ^D_{ML}/τ^D_{BL} for the donor decays in the monolayer and bilayer configurations. Results in panel (b) are for the SiO_2 substrate with a refraction index $n_G = 1.5$, results in panel (c) are for the Si substrate whose complex dielectric function at the emission wavelength $\lambda_0 = 545$ nm is as reported by Aspnes and Studna.[6,21] Each panel features results calculated for two different distances z of 4 and 5 nm, and for two different values of $n = 2$ and 2.5 as indicated. Also shown in panels (b) and (c) are the corresponding coordinated ET efficiencies into the A layer defined as a fraction of the overall decay into all channels (upper curves referring to the right axes). d) ET efficiency from donor NQDs into the Si substrate in the bilayer configurations. Different style curves are coordinated with the lines in panel (c). The lower group of curves shows the direct ET into Si as a fraction of the donor decay into all channels. For the total ET (the upper group of curves), the direct ET is complemented by the sequential ET process via the acceptor layer. Here, the efficiency of the ET into the acceptor layer is taken from panel (c), and 90% of the acceptor excitons are assumed[6] to be further transferred into Si.

The results of Figure 3 yield a value of $a \cong 1.4 \times 10^4$ cm^{-1} at the donor emission wavelength $\lambda_0 = 545$ nm. We consider this value only as representative—we are not pursuing actual fits with the computational data in this paper and rather concentrate on semi-quantitative understanding. Overall, the experimentally observed value of $\tau^D_{ML}/\tau^D_{BL} \cong 11.4$ on SiO_2 substrates (Figure 1) can be rationalized in the context of computational results in Figure 2b, particularly given the fact that extra dielectric screening takes place in experimental samples due to the presence of the donor layer, which is absent in the model system. The same theoretical panel (b) also shows that the ET efficiency into the acceptor layer is very high, in excess of 80% for all the curves shown and at or above 90% in the expected experimental region. Here, efficiency is defined as a fraction of the overall decay rate of the donor exciton. Indeed, the rate of NRET into the A layer here should dominate with respect to the rates of otherwise radiative processes. The latter are only modestly accelerated from the spontaneous vacuum value in the vicinity of SiO_2 substrates: the computations yield $\tau_1/\tau_0 \cong 1.63$ at $z = 4$ nm and $\tau_1/\tau_0 \cong 1.55$ at $z = 10$ nm. This weak distance dependence of the radiative processes has already been mentioned earlier in this paper.

On the other hand, the exciton decay is expected to be greatly affected in the vicinity of Si substrates: the computations give $\tau_1/\tau_0 \cong 9.96$ at $z = 4$ nm, which reduces to $\tau_1/\tau_0 \cong 6.95$ at $z = 5$ nm and falls to $\tau_1/\tau_0 \cong 3.63$ at $z = 10$ nm. The main reason for this strong distance dependence is that NRET into Si is a very substantial contributor whose rate drops precipitously within several nanometers.[5–8] However, even weakly distance-dependent RET process have much higher rates into Si than into SiO_2 due to higher refraction index of Si. With stronger competition from ET into Si, the ET efficiency for the

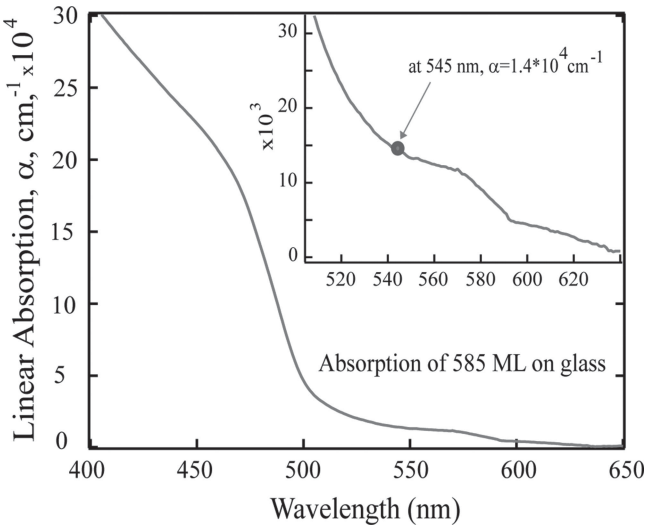

Figure 3. The wavelength dependence of the effective absorption coefficient of the acceptor layer as derived from the measured raw data on optical density of the monolayer of acceptor NQDs under the assumption of layer thickness of 5 nm.

donor exciton into the A layer should be lower on Si substrates than on SiO_2 substrates. This is quantitatively illustrated in Figure 2c. The computational data in this panel suggests that the ratio τ^D_{ML}/τ^D_{BL} of the decay rates in the monolayer and bilayer configurations on Si substrates should be substantially smaller than that measured on SiO_2 substrates: for this model, we expect values within the 2–3 range.

Comparison of the experimental data for the monolayer and bilayer configurations on Si substrates is shown in **Figure 4**. Similar to samples on SiO_2 substartes, the PL intensity of the donor emission in bilayers on Si is strongly reduced in comparison with the acceptor emission (Figure 4b). The quantitative results for samples on Si substrates are however quite different from samples on SiO_2 substrates. First, the donor decay time in the monolayer configuration on Si is much faster (Figure 4c): $\tau^D_{ML} \cong 3.3$ ns, about 6.2 times as fast as the decay in monolayers on SiO_2. This agrees well with our previous measurements[6] at the donor wavelength and the computational results from the model system. The acceleration of the decay is caused by the combined effects of NRET and RET into the Si substrate.[5,7] Second, an even faster donor decay is observed in the bilayer samples: $\tau^D_{BL} \cong 1.1$ ns (the value is derived from a double exponential fit to the decay curve in Figure 4c), but the ratio of the decay times: $\tau^D_{ML}/\tau^D_{BL} \cong 3$, is now substantially smaller than the value obtained for the samples on SiO_2 substrates. With a single exponential fit to the decay curve, the extracted value $\tau^D_{BL} \cong 1.6$ ns results in an even smaller ratio $\tau^D_{ML}/\tau^D_{BL} \cong 2.1$. These smaller values are very much in line with the theoretical expectations of the τ_1/τ_2 ratio shown in Figure 2c for the model system. As discussed above, the smaller ratio is a result of a decreased ET rate from the donor into the Si substrate in the bilayer configuration: at such distances from the substrate, NRET does not add significantly to the RET contribution. (For smaller distances from the donor to the Si substrate in the monolayer configuration, NRET is a major decay channel.) On the other hand, NRET from donor NQDs into the acceptor layer would have practically the same rate w on either substrate—if no changes in the acceptor layers exist—and it is tempting to use the information extracted from samples on SiO_2 substrates for the analysis of the experimental data on Si substrates. Equating the donor decay rate $\gamma^D + w$ in Equation (3) with the observed inverse decay time $1/\tau^D_{BL}$ in the bilayer configuration and taking $\tau_w \cong 2.0$ ns from measurements on SiO_2, one would arrive at the efficiency $w/(\gamma^D + w)$ of ET into the acceptor layer equal to ≅ 55% for $\tau^D_{BL} = 1.1$ ns and ≅ 80% for $\tau^D_{BL} = 1.6$ ns. While the former efficiency estimate appears too low to be consistent with the model predictions in Figure 2c, the latter estimate is in good agreement with the range of expectations from the model guidelines. The self-consistency of the second estimate can further be verified by evaluating the rate $\gamma^D = 1/\tau^D_{BL} - 1/\tau_w$ and comparing it to the rate $\gamma^D_{ML} = 1/\tau^D_{ML}$, where we find $\gamma^D_{ML}/\gamma^D \cong 2.4$ for $\tau^D_{BL} = 1.6$ ns, a very reasonable ratio from the theoretical view point. On the other hand, if $\tau^D_{BL} = 1.1$ ns is used with the same values of w and τ^D_{ML} that would lead to an obviously incorrect value γ^D_{ML}/γ^D. Given the variations in linkers and grafting procedures on different surfaces, some variations in the acceptor layers on different substrates are possible, and then the interlayer NRET rate w could be somewhat different in the configurations on SiO_2 and on Si. With these uncertainties, it appears unwarranted at this stage to look for a more detailed quantitative agreement with the computational results obtained for an approximate model system.

We further ascertain ET from the donor to the acceptor layer by comparing the acceptor PL kinetics curves. Figure 4d and its inset clearly show a delayed rise time of the acceptor PL in the bilayer configuration – as expected from Equation (4). As we discussed above, the evolution of the PL dynamics curves can strongly depend on the interplay of the kinetic rates (w, γ^A) as well as on the initial ratio $N_D(0)/N_A(0)$ of photogenerated excitons. With much higher decay rates on Si substrates, the resulting decay of the acceptor PL is much faster, which often complicates a quantitative delineation of the rise and fall pattern; however, a delayed rise-time pattern is still clearly observed for the bilayer configuration. Additionally, a visually satisfactory fitting can be done, as the inset shows for the particular fit that resulted in the values of $N_D(0)/N_A(0) \cong 2.4$ and $\tau_w \cong 3$ ns. While these may be reasonable estimates by themselves, their precise quantitative consistency with the donor-decay results is not as clear and we do not rely on them for any firm quantitative conclusions. Once again, this may be reflective of the delicate nature of the linking and grafting procedures that may result in variations between different samples. However, it is reassuring that the kinetic parameters derivable from different fitting routines appear to be within reasonable variation ranges. As an example, different estimates that we extracted for interlayer NRET rates in different samples vary at most by a factor of 2.

Just as in the case for samples on SiO_2 substrates, we stress that the decay times for acceptors in the monolayer and bilayer configurations on Si surface are evidently very close to each other, see Figure 4d. Moreover, they are close to the donor decay times and to our earlier results[6] for the submonolayer samples. This indicates that the grafting and linking procedures we used allowed us to avoid the formation of any appreciable number of energy trapping and scavenging sites, otherwise the

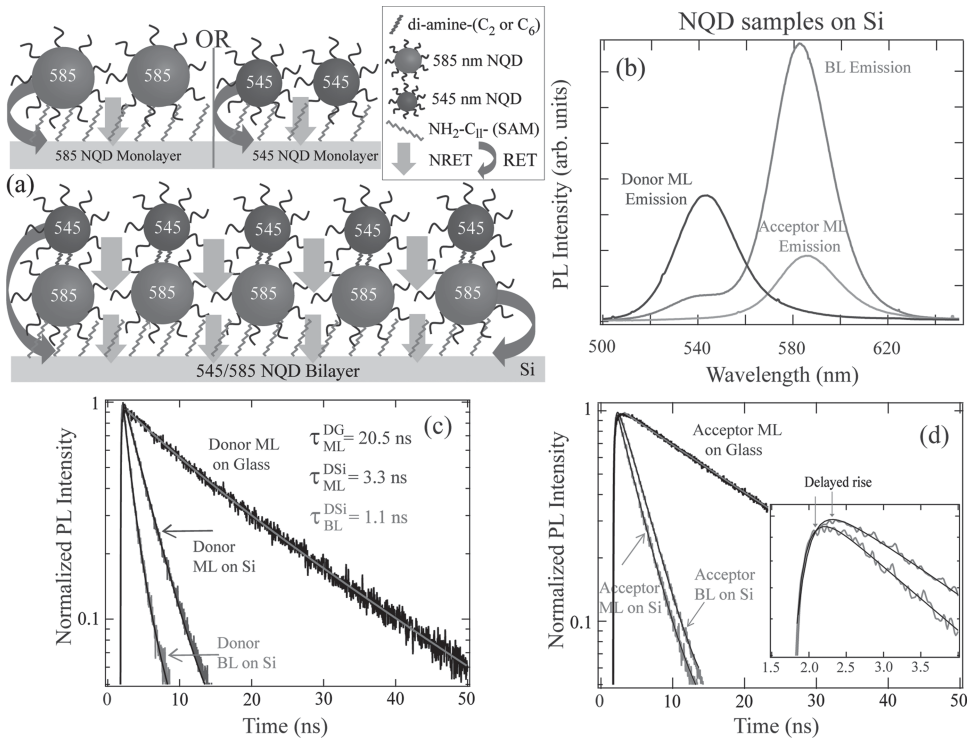

Figure 4. a) Schematics of the monolayer and bilayer NQD placements and of the relevant ET processes on Si substrates. b) PL emission spectra of donor monolayer (NQD-545, ML), acceptor monolayer (NQD-585, ML) and bilayer (NQD-545 on NQD-585, BL) samples grafted on the Si substrates. c) Compared are the PL dynamics at the donor emission peak (545 nm) for the donor monolayer on SiO_2 (top trace), donor monolayer on Si (middle trace) and donor in the bilayer on Si (bottom trace) configurations. Traces are shown along with the fitting curves. d) Comparison of the PL kinetics at the acceptor emission peak (585 nm): acceptor monolayer on SiO_2 (top trace), acceptor monolayer on Si (bottom trace), and acceptor in the bilayer on Si (middle trace). The inset more clearly shows the delayed rise time and the fitting curves.

PL lifetimes would have become even shorter due to additional PL quenching channel(s). In support of this conclusion is the rather faithful correspondence between experimental data and theoretical expectations from the simple model system that does not invoke any detrimental energy scavenging processes but incorporates only well-characterized radiative and non-radiative processes of ET and photon emission.

The experimental data we obtained can thus allow for full rationalization on the basis of well-defined ET pathways without a need to invoke poorly characterized non-radiative exciton trapping/scavenging mechanisms discussed for NQD solids. The good correspondence between our experimental observations and the theoretical expectations from the simple model system in Figure 2 suggests to use the model's help in the further analysis. We are particularly interested in the efficiency of ET from the donor NQDs into the Si substrate in the bilayer configuration, an important measure for photovoltaic applications. Figure 2c shows the efficiency of NRET from the donor exciton into the acceptor layer as a fraction of the overall donor decay. Consistent with our experimental data for the bilayers on Si substrates, it is clear that the majority of the photoexcitations created in the donor NQD layer are first transferred into the acceptor NQD layer, the precise quantity being dependent on values of system parameters. In addition, a portion of the donor excitons are transferred directly into the Si substrate. At this distance ≈10 nm from the substrate, this direct ET is mainly realized via the longer-range RET coupling but there is still some contribution from NRET.[5,6,8] The lower group of curves in Figure 2d shows the computational results for the efficiency of the direct ET as fraction of the overall donor decay. The precise quantity here is also evidently dependent on the values of the system parameters. The excitons that are first transferred into the A layer would, in turn, be efficiently transferred into the Si substrate via the combined effects of NRET and RET[5,6] from the acceptor NQDs. Our prior studies[6] showed that the efficiency of this ET is close to 90%. Using this number we calculate the total efficiency of direct and sequential ET from donor NQDs into Si shown in Figure 2d as the upper group of curves. These curves are nearly on top of each other and remarkably display an efficiency approaching 90% with practically no dependence on the system parameters. The assumption of 85% efficiency of ET from the acceptor NQDs into Si results in the total ET efficiency close to 85% and also showing very little dependence on the values of system parameters.

Figures 2c and 2d illustrate that the weakly varying total efficiency can be seen as a result of the complementary characters of the direct and sequential processes. This can also be understood from another viewpoint: by recalling that the only losses for ET in our model correspond to NQD excitons decaying via photon emission, the process responsible in particular for the PL used in experimental measurements. The photon emission process is suppressed in the vicinity of the interface and is only weakly distance-dependent at the distances studied. In fact, approximately half of such photons[8] would be emitted in the direction

of Si and additionally absorbed in thick enough substrates. We however follow our definition of ET in references[5,6] and do not include such photons in the calculation of radiative ET efficiency. The efficiency of ET into Si is thus evaluated as only due to near fields (NRET and RET into evanescent/waveguiding modes) that would be applicable even for ultrathin substrates.[5]

3. Conclusion

In this work, we have extended our grafting and linker-assisted strategies to fabricate dense NQD bilayers on Si and SiO_2 substrates. We performed a detailed comparative study of the NQD PL decays in monolayer and bilayer configurations. Our experimental results and their good agreement with theoretical expectations from a basic electrodynamics model indicate that the resulting NQD structures do not possess any appreciable number of exciton/energy scavenging defects. We also showed that bandgap-gradient NQD structures can assist in efficient directional "funneling" of NQD excitons into the underlying Si substrate. This demonstration of very efficient (nearly 90%) ET into Si from the outer NQD layer in the bilayer configuration complements our earlier findings of highly efficient ET from the proximal NQDs to validate the concept of excitonic sensitization of ultrathin Si layers from the adjacent NQD assemblies.

The efficacy of the fabrication approach we used is expected to be maintainable in building multi-layer optically thick NQD solids with little or no energy scavenging losses. It is conceivable that high efficiencies of overall ET from such multi-layer structures into Si substrates are possible to achieve by further enhancing the interlayer NRET through appropriate linking and optimization of the bandgap-gradient NQD structures. ET processes and efficiencies could likely be improved by utilizing NQDs of various compositions and sizes. The reported results thus further support our proposition that NQD/Si nanostructures are attractive materials systems for practical realization of energy-transfer-based thin-film photovoltaic devices.

4. Experimental Section

Functionalization of Si and SiO_2: Silicon (<111>, CZ, P/Boron, 1–10 Ωcm^{-1}) and silicon oxide (2 μm SiO_2 on <100> Si) were used as substrates in the experiments. SiO_2 wafers were prepared by thermal oxidation in a cleanroom environment using silicon tetrachloride and molecular oxygen. The wafers were degreased via 10 min sequential sonication in dichloromethane, acetone, and methanol followed by rinsing in Milli-Q water (resistivity 18 $M\Omega cm^{-1}$). Si wafers were further cleaned following standard RCA procedures[26] while the SiO_2 wafers were cleaned in a Piranha solution (composed of a 1:4 mixture of concentrated H_2O_2:H_2SO_4) at 85 °C for 30 min. Amine functionalized Si and SiO_2 surfaces were prepared as previously described.[27] In brief, oxide-free Si surfaces were prepared by etching with 49% HF for 1 min 30 s, followed by 15 min in 40% NH_4F, resulting in an atomically smooth hydrogenated substrate. An ester terminated monolayer was prepared using standard Schlenk line techniques by immediately inserting the freshly etched Si wafer into ethyl undecylenate at 200 °C for 4 h under argon flow. The ester groups were transformed into carboxyl groups through deprotection with potassium tert-butoxide in DMSO (0.25 M, for 90 s, and then rinsed in DMSO) followed by protonation with HCl (2 M, for 1 min, and then rinsed in H_2O). Ethylene-diamine was grafted to the carboxylic acid group in a solution of 1-ethyl-3-(3-dimethylaminopropyl) carbodiimide (EDC) buffered in 2-(*N*-morpholino)ethanesulfonic acid (MES)[5,7,11] using well known EDC coupling techniques at room temperature resulting in amine termination. Amine terminated SiO_2 wafers were prepared in a 0.2 wt.% solution of 11-aminoundecyltriethoxy silane (AUTES) at 70 °C for 12 h in a nitrogen glovebox.

Grafting of QDs on Amine-Terminated Surfaces: Organic capped CdSe/ZnS core shell NQDs emitting at $\lambda_0 \simeq 545$ nm and $\lambda_0 \simeq 585$ nm were purchased from Invitrogen Life Sciences (5nM, dispersed in n-decane, 5nM) and used as received. NQDs were grafted to the amine terminated surfaces by immersing samples in a dilute NQD solution in hexane (7 or 20 μL NQDs in 2 mL hexane for submonolayer or monolayer coverage, respectively) for 2 h. The samples were rinsed twice with toluene and then immersed either in an 15mM solution of 1,6-hexanediamine or ethylenediamine in toluene for 1 h to passivate the NQDs interface. Monolayer samples were rinsed twice in toluene and dried under the N_2 gas. Bilayer samples were prepared by repeating the NQD attachment and passivation process. Specifically, a freshly prepared dense monolayer of 585 nm NQDs on Si or SiO_2 substrates treated with diamine was immersed in a solution of 545 nm NQDs (7 to 20 μL NQDs in 2 mL hexane) and left for 2 h before rinsing and surface passivation. All samples were stored under N_2 prior to spectroscopic measurements.

Spectroscopic Analysis: For spectroscopic studies, we used a microscope-based time-resolved PL system. Samples were mounted on the microscope table and excited at 405 nm by 50 ps laser pulses at 2.5 MHz from a Picoquant diode laser. Excitation was focused on the sample via a NA = 0.6 objective that also ensured a high photon collection efficiency necessary to obtain PL signatures from monolayers of NQDs. The collected emission was passed through a spectrometer and directed to either a CCD camera for spectral analysis or a sensitive photon detector (MicroPhoton Devices) for the wavelength-dependent PL lifetime detection. PL decays were collected *via* the time-correlated single photon counting (TCSPC) performed on board of Pico300E photon counting hardware (PicoQuant GmbH). The overall time resolution was better than 70 ps.

Acknowledgements

We are grateful for the support of this work provided by the DOE/BES grant (DE-SC0010697). We thank H. M. Nguyen and O. Seitz for their assistance and useful discussions in the beginning of this work. A. V. M. thanks H. Htoon from CINT/LANL for enlightening discussions.

Received: February 26, 2014
Revised: March 27, 2014
Published online: May 26, 2014

[1] R. R. Lunt, T. P. Osedach, P. R. Brown, J. A. Rowehl, V. Bulović, *Adv. Mater.* **2011**, *23*, 5712.
[2] C. R. Belton, G. Itskos, G. Heliotis, P. Stavrinou, P. Lagoudakis, J. Lupton, S. Pereira, E. Gu, C. Griffin, B. Guilhabert, I. M. Watson, A. R. Mackintosh, R. A. Pethrick, J. Feldmann, R. Murray, M. D. Dawson, D. D. C. Bradley, *J. Phys. D: Appl. Phys* **2008**, *41*, 094006.
[3] V. M. Agranovich, Y. N. Gartstein, M. Litinskaya, *Chem. Rev.* **2011**, *111*, 5179.
[4] B. Ke, *Photosynthesis: Photobiochemistry and Photobiophysics*, Kluwer, New York, **2001**.
[5] H. M. Nguyen, O. Seitz, W. Peng, Y. N. Gartstein, Y. J. Chabal, A. V. Malko, *ACS Nano* **2012**, *6*, 5574.
[6] M. T. Nimmo, L. M. Caillard, W. D. Benedetti, H. M. Nguyen, O. Seitz, Y. N. Gartstein, Y. J. Chabal, A. V. Malko, *ACS Nano* **2013**, *7*, 3236.

[7] H. M. Nguyen, O. Seitz, D. Aureau, A. Sra, N. Nijem, Y. N. Gartstein, Y. J. Chabal, A. V. Malko, *Appl. Phys. Lett.* **2011**, *98*, 161904.
[8] H. M. Nguyen, O. Seitz, Y. N. Gartstein, Y. J. Chabal, A. V. Malko, *J. Opt. Soc. Am. B* **2013**, *30*, 2401.
[9] S. Chanyawadee, R. T. Harley, M. Henini, D. V. Talapin, P. G. Lagoudakis, *Phys. Rev. Lett.* **2009**, *102*, 077402.
[10] S. Lu, Z. Lingley, T. Asano, D. Harris, T. Barwicz, S. Guha, A. Madhukar, *Nano Lett.* **2009**, *9*, 4548.
[11] O. Seitz, L. Caillard, H. M. Nguyen, C. Chiles, Y. J. Chabal, A. V. Malko, *Appl. Phys. Lett.* **2012**, *100*, 021902.
[12] D. V. Talapin, J. Lee, M. V. Kovalenko, E. V. Shevchenko, *Chem. Rev.* **2010**, *110*, 389.
[13] A. H. Ip, S. M. Thon, S. Hoogland, O. Voznyy, D. Zhitomirsky, R. Debnath, L. Levina, L. R. Rollny, G. H. Carey, A. Fischer, K. W. Kemp, I. J. Kramer, Z. Ning, A. J. Labelle, K. W. Chou, A. Amassian, E. H. Sargent, *Nat. Nanotechnol.* **2012**, *7*, 577.
[14] C. R. Kagan, C. B. Murray, M. G. Bawendi, *Phys. Rev. B* **1996**, *54*, 8633.
[15] C. Dang, J. Lee, C. Breen, J. S. Steckel, S. Coe-Sullivan, A. Nurmikko, *Nat. Nanotechnol.* **2012**, *7*, 335.
[16] M. Achermann, M. A. Petruska, S. Crooker, V. I. Klimov, *J. Phys. Chem. B* **2003**, *107*, 13782.
[17] T. Franzl, T. A. Klar, S. Schietinger, A. L. Rogach, J. Feldmann, *Nano Lett.* **2004**, *4*, 1599.
[18] T. A. Klar, T. Franzl, A. L. Rogach, J. Feldmann, *Adv. Mater.* **2005**, *17*, 769.
[19] W. Peng, O. Seitz, R. A. Chapman, E. M. Vogel, Y. J. Chabal, *Appl. Phys. Lett.* **2012**, *101*, 051605.
[20] V. M. Agranovich, M. D. Galanin, *Electronic Excitation Energy Transfer in Condensed Matter*, Elsevier, Amsterdam, **1982**.
[21] D. E. Aspnes, A. A. Studna, *Phys. Rev. B* **1983**, *27*, 985.
[22] R. R. Chance, A. Prock, R. Silbey, in *Advances in Chemical Physics Vol. 37*(Eds: S. A. Rice, I. Prigogine), Wiley, New York, **1978**, pp 1.
[23] L. Novotny, B. Hecht, *Principles of Nano-Optics*, Cambridge University Press, Cambridge, **2006**.
[24] K. Roodenko, H. M. Nguyen, L. Caillard, A. Radja, P. Thissen, J. M. Gordon, Y. N. Gartstein, A. V. Malko, Y. J. Chabal, *J. Phys. Chem. C* **2013**, *117*, 20186.
[25] J. M. Gordon, Y. N. Gartstein, *J. Phys.: Condens. Matter* **2013**, *25*, 425302.
[26] W. Kern, *J. Electrochem. Soc.* **1990**, *137*, 1887.
[27] O. Seitz, M. Dai, F. S. Aguirre-Tostado, R. M. Wallace, Y. J. Chabal, *J. Am. Chem. Soc.* **2009**, *131*, 18159.